

# Mapping the dark matter distribution at high redshift with NGST

Program contacts: Peter Schneider, Jean-Paul Kneib, Roser Pelló  
Scientific category: DISTANT GALAXIES  
Instruments: OPT/CAM, NIR/CAM  
Days of observation: 192

## Abstract

Applying recently developed weak gravitational lensing techniques to ultra-deep multi-band images as routinely obtained by NGST, the (dark) matter distribution at high redshift shall be studied on scales ranging from individual galaxies, through groups and clusters, up to the large-scale matter distribution in the Universe on scales below about 3 Mpc. Redshift estimates from multiple colors will allow to study the massive properties of galaxies as a function of redshift, luminosity, morphology, and environment, and will be able to probe the redshift-dependence of scaling relations (such as Tully-Fischer). The precise determination of the masses of high-redshift clusters will provide strong constraints on the evolution of structure, and the same techniques will allow the detection of clusters from their massive properties only, yielding an accurate mass-selected sample of clusters at various epochs which can be compared directly with cosmological predictions. Measuring the cosmic shear on scales of about ten arcminutes will reveal the (highly non-Gaussian) statistical properties of the dark matter distribution, as a function of redshift, and thus probes regimes not observable through the CMB experiments. The data requested here will yield unprecedented strong lensing results for cosmological applications. The unique ability of NGST to obtain high-quality resolved images of galaxies at very high redshift is essential for the scientific goals of this proposal.

*All data obtained here are also useful for a number of other science projects. In particular, two of the three major science goals require random high-latitude fields, which can be selected in accord with the scientific requirements of other proposals.*

**NOTE: The required observing time is strictly inversely proportional to the detector area; changing to an 8 arcminute field will cut all time estimates by a factor of 4.**

ASWG DRM Proposal  
Mapping the dark matter distribution at high redshift with NGST

**Observing Summary:**

Target	RA	Dec	$K_{AB}$	Configuration/mode	Days
RANDOM FIELDS AT HIGH GALACTIC LATTITUDE	xxx	xxx	$K \lesssim 29$	OPT/CAM, NIR/CAM	65
SELECTED FIELDS AT HIGH GALACTIC LATTITUDE	xxx	xxx	$K \lesssim 27.5$	OPT/CAM, NIR/CAM	60
RANDOM FIELDS AT HIGH GALACTIC LATTITUDE	xxx	xxx	$K \lesssim 26.8$	OPT/CAM, NIR/CAM	67
Grand total days					192

**NOTE:** The required observing time is strictly inversely proportional to the detector area; changing to an 8 arcminute field will cut all time estimates by a factor of 4.

## ■ Scientific Objectives

Ultra-deep observations with NGST will reveal the distribution and the physical properties of very high-redshift galaxies. Precursors of our present-day galaxies can be studied with unprecedented accuracy, exploring regions of parameter space (redshift, luminosity, morphology, size) which are currently unknown. The remaining link between these new insights into the evolution of galaxies and structure formation (and cosmology) is the relation between optical/IR properties of galaxies and the mass of the halo in which they are embedded as a function of cosmic time. Bridging this gap between the luminous properties of matter concentrations and modelling of the formation of structure is essential for our understanding of the evolution of galaxies, groups, and clusters, and that of the Universe as a whole.

Gravitational lensing is probably the only method that will provide the missing link. Probing the tidal gravitational field of mass concentrations (or, more generally, of the intervening mass distribution) by the distortion of light bundles originating from background galaxies, the mass of galaxies, groups, and clusters can be determined individually, or statistically.

This weak gravitational lensing effect has been studied in great detail recently, and applied successfully to several (classes of) systems; in particular, the projected (dark) matter distribution of several medium-redshift clusters of galaxies has been reconstructed, using both parametric and parameter-free approaches, and the mass and physical scale of galaxy halos have been constrained statistically, employing the so-called galaxy-galaxy lensing effect. Furthermore, clusters of galaxies have been detected from observing their tidal gravitational field through the image distortion of faint background galaxies, thus allowing to define a sample of clusters from their mass properties only (i.e., without referring to their luminous properties).

In addition to weak lensing applications, the data requested in this proposal will also be of tremendous value for strong lensing, detecting hundreds of multiple image systems caused by individual galaxies, and a wealth of strong lensing features in clusters of galaxies which will allow to determine their central mass distribution with unprecedented accuracy and resolution.

As demonstrated by HST, deep high-resolution images are critical in lensing studies (e.g. Kneib et al 96, Smail et al 96, Seitz et al 96). The unique NGST capabilities in terms of spatial resolution and sensitivity, as well as the opening of the 2-5 $\mu$ m window, will benefit lensing studies at high redshift. A completely new and accurate view on the dark mass distribution in the Universe is thus expected.

We propose the following 3 NGST main weak-lensing science programs based on deep multi-waveband images:

### **(A) Statistical Properties of the Dark Matter Halos of Galaxies:**

Employing the method of galaxy-galaxy lensing, the parameters of mass models for galaxies can be determined (Brainerd et al 1996; Griffiths et al 1997; Hudson et al 1998). Such a model should contain (at least) a mass scale and a length scale. Making use of the large area covered, the depth in redshift, and the expected accurate photometric redshift estimates,

the galaxy sample can be ‘sliced’ into luminosity, redshift, color, and morphology. Using maximum-likelihood techniques (Schneider & Rix 1997; Geiger & Schneider 1998b), this will allow to study: i) the evolution of halo mass and size with redshift (at fixed luminosity), ii) the evolution of the Tully-Fisher-like scaling relations, and their dependence on environment (field galaxies vs. galaxies in pairs vs. cluster/group galaxies; see Natarajan & Kneib 1997; Geiger & Schneider 1998a,b; Natarajan et al 1998).

Combining these results on halo masses with the optical/IR properties of galaxies, the missing link between dark matter and light distribution can be provided up to very high redshift. Indeed, mapping  $\sim 0.18\text{deg}^2$  down to  $K \sim 29$ , (to obtain a high number density of  $\sim 5 \times 10^6 \text{ deg}^{-2}$  background galaxies with sufficiently large redshift – see justification in Observing Strategy) will allow to determine the mass parameters of (mainly field) galaxies up to  $K \sim 24$  and beyond, and therefore to cover a broad range in redshift (up to  $z \sim 5$ ) and in luminosity. To obtain accurate photometric redshift estimates for most galaxies, similarly deep images in four other band are required.

**(B) Evolution of the Mass Distribution of High-Redshift Clusters/Groups:**

Matched-filter analyses of the galaxy distribution (from 10-m ground-based telescopes or shallow NGST surveys), future X-ray deep surveys (AXAF/XMM), SZ observations (MAP/-Planck) will likely discover a large number of cluster/proto-cluster candidates at redshift much beyond one. From a cosmological point of view, it is essential to understand the *mass* properties of these clusters and the mass function evolution with time, to compare with Press-Schechter-like predictions. With NGST, medium-redshift clusters with a velocity dispersion in excess of  $\sim 300 \text{ km/s}$  and high-redshift clusters with  $\sigma_v \gtrsim 500\text{km/s}$  can be significantly detected individually from their corresponding distortion map (Miralda-Escudé 1990; Schneider 1996). For lower-mass clusters and groups, we have to statistically combine the signal. In the former case, the fraction of genuine high-redshift clusters within the candidate list can be obtained, in the latter case, the abundance of such clusters can be studied. As high-redshift clusters are not expected to be in dynamical equilibrium, the lensing mass estimates are even more important than for low-redshift clusters. The projected mass distribution of clusters with larger mass can be mapped in detail to study the morphology and the amount of substructure, and its relation to the galaxy distribution (Kaiser & Squires 1993, Seitz & Schneider 1995, 1996, 1998; Squires et al 1996a,b, 1997; Seitz et al 1996; Hoekstra et al 1998).

Furthermore, from the list of cluster candidates, pairs (or groups) of cluster will be selected and imaged deeply with NGST, to search for matter filaments connecting these pairs which are predicted in most scenarios of structure formation. We shall determine the mass distribution of about 50 clusters with a broad distribution in redshift up to  $z \sim 2.5$ , and selected by various of the aforementioned methods, in order to study their total mass, their dynamical state, to see whether merging of halos can be ‘caught in the act’, and to search for larger-scale massive structures connected to these clusters. To separate foreground- and background galaxies, and faint cluster members, images in five wavebands will be taken, covering a square of 8 arcminutes (roughly corresponding to  $1h^{-1}\text{Mpc}$  radius) around each cluster.

**(C) Statistical Properties of the Dark Matter Distribution in the Universe:**

The statistical properties of the distortion field of the images of high-redshift galaxies directly reflect the statistical properties of the intervening mass distribution. For example, the two-point ellipticity statistics (such as rms inside circular apertures or correlation functions) depend directly on the appropriately weighted and projected power spectrum of the cosmic mass distribution (Blandford et al 1991; Kaiser 1992, 1998; Jain & Seljak 1997; Schneider et al 1998; Seljak 1998). Whereas the large-scale power spectrum on comoving scales  $\gtrsim 10h^{-1}\text{Mpc}$  will have been measured by MAP and PLANCK, the cosmic shear measures the mass distribution on much smaller scales and at a non-linear stage. A comparison with the linear power spectrum then yields strong constraints on the evolution of the mass distribution, e.g., that of the power spectrum, at relatively late epochs. The gravitational instability picture of structure formation can therefore be tested with high accuracy. In addition, these observations will also be used to define a mass-selected sample of clusters (Schneider 1996), and in particular might find cluster-mass halos which are very underluminous and therefore missed in standard cluster searches ('dark clusters'). Ongoing and planned deep wide-field imaging surveys will measure the power spectrum and the halo abundance for typical redshifts of about 0.5; the present proposal aims at extending this to redshifts of order 2 or 3 which requires a much higher number density of background galaxies and a considerably higher mean redshift for them. By comparing the projected dark matter distribution, statistically sliced into redshift bins according to the (magnitude-dependent) redshift distribution of the background galaxies (Seljak 1998), with the galaxy distribution at  $z \lesssim 3$ , the redshift- and scale dependence of the bias 'factor' can be studied in great detail (Schneider 1998; van Waerbeke 1998). For example, to obtain a statistically significant sample of  $\sim 500$  halos detected from their mass properties only (cf. Kruse & Schneider 1998; this number is strongly dependent on the cosmological model), a total area of  $\sim 5\text{deg}^2$  should be mapped down to  $K \sim 27$ . Given that for such high redshifts the 'dark halo confusion limit' is reached (cf. the simulated shear maps by Jain et al 1998), photometric redshift information of the *background* galaxies is essential to distinguish the tidal gravitational field of several mass concentrations along the same line-of-sight, using the redshift dependence of the lens effect.

We therefore propose to carry out 3 imaging surveys with NGST, with specifications motivated by each of the three science programs listed above:

**(I) Very Deep Imaging Survey (VDIS).** An area of  $0.18 \text{ deg}^2$  shall be mapped down to  $K = 29$  at a S/N of 5, requiring an exposure time of about 27600 sec, and with similar exposure time in four other wavebands, yielding (at a S/N of 3)  $V \sim 30.5$ ,  $I \sim 30.3$ ,  $H \sim 29.8$ ,  $M \sim 27.8$ . The multi-color information should enable the determination of accurate photometric redshifts, dividing the sample into classes of galaxies ('early' vs. 'late'-type objects), and to allow for the detection of larger-scale mass concentrations such as groups and clusters from color-magnitude diagrams.

**(II) Cluster Deep Imaging Survey (CDIS).** For 50 medium- and high-redshift clusters and cluster candidates, selected either through optical/X-ray or SZ or from the WFIS survey described below, fields of  $8 \times 8$  arcminutes around the cluster 'centers' should be mapped down to  $K = 27.5$  at S/N of 5. The sample of 50 is an absolute minimum

in order to cover a wide range in redshift, ‘richness’, and method of primary selection. In addition, imaging in four other wavebands with the same exposure time will yield (at a S/N of 3)  $V \sim 29$ ,  $I \sim 28.8$ ,  $H \sim 28.3$ ,  $M \sim 26.3$ . The scientific rationale for multi-colors is the same as described before; in addition, the identification (from color-magnitude diagrams) of very faint cluster members is essential to delineate the optical appearance of the clusters and compare it with the mass distribution.

**(III) Wide Field Imaging Survey (WFIS).** A total of  $\sim 5\text{deg}^2$  shall be mapped down to  $K = 26.7$  at a S/N of 5, requiring an exposure time of about 1200 sec, and with similar exposure time in four other wavebands, yielding (at a S/N of 3)  $V \sim 28.2$ ,  $I \sim 28$ ,  $H \sim 27.5$ ,  $M \sim 25.3$ . The scientific rationale for multi-colors is the same as described before.

In estimates the exposure time we have assumed that the weak lensing studies will be primarily carried out with the K-band images. Of course, with the images in the other four bands having comparable depth (in terms of number density of faint galaxies), they too will be used for weak lensing, thus providing an important cross-check for the stability and reliability of the results; also, particular subsets of background galaxies may appear at larger S/N and/or smaller intrinsic ellipticity distribution than that in the K-band, and may be more appropriate for deriving accurate mass profile estimates for specific lens redshifts.

Science program (A) will use primarily the VDIS. However, the WFIS provides ample statistics for a detailed investigation of the mass profiles of somewhat brighter ( $K \sim 23$ ) galaxies at somewhat lower redshifts ( $z \lesssim 3$ ). The CDIS will be used to investigate the dark halo properties of galaxies in cluster at various redshifts, e.g., to see how their dark halo has been stripped and at what redshift this typically occurs (e.g., Moore et al 1998; Tormen et al 1998).

Science program (B) will mainly make use of the CDIS. However, the mass maps of the more massive clusters detected in the WFIS will also be amenable to detailed mass map reconstructions.

Science program (C) will use mainly the VDIS and WFIS, to measure cosmic shear, and thus the statistical properties of the dark mass distribution, on scales from  $\sim 5$  arcseconds to  $\sim 30$  arcminutes. The VDIS will primarily be used for the highest-redshift distributions, up to  $z \sim 4$ , whereas the WFIS can study the distribution up to  $z \sim 2$  or 3 in great detail. The dark halo search in both surveys will also be distinguished by redshift; in addition, in the CDIS, dark halo companions of otherwise identified clusters are expected to show up, allowing the study of merger processes at high redshifts.

**Spin-offs regarding strong lensing:**

Whereas these surveys are designed according to the requirements of weak lensing applications, they will also be extremely useful for strong lensing applications. Given the depth of images routinely obtained with NGST, these exposures will contain several strong lensing systems, where a high-redshift faint galaxy will be mapped into two or more images by a foreground galaxy, thus allowing an accurate estimate of the mass of the latter. Note that several such candidate multiple image systems have been found in the MDS (Ratnatunga et al 1995) and in the HDF (Hogg et al. 1996). The probability of a given source at high redshift to be multiply imaged depends on the evolution of the halo abundance, but is typically a

few  $\times 10^{-4}$ . With a number density of  $\sim 600 \text{arcmin}^{-2}$ , and a field of view of  $\sim 16 \text{arcmin}^2$ , observing multiply imaged galaxies in virtually every NGST image is certain. To identify them, the high angular resolution of NGST to find morphologically similar galaxy images will be of utmost importance, together with multi-color information. The same observations required for the weak lensing programs mentioned above will then be useful to constrain the halo abundance on mass scales down to a few  $\times 10^9 M_\odot$  as a function of redshift. The statistics of strong lensing events is an extremely powerful tool to study the geometry of the Universe, and the (mass) evolution of the galaxy population (e.g., Kochanek 1993, 1995; Maoz & Rix 1993), and an NGST lens sample will easily become the most useful one for this purpose, increasing the total number of lens systems by more than an order of magnitude – all of them with photometric redshift estimates of source and lens.

Deep imaging of relatively low-redshift clusters will also be extremely useful for strong-lensing applications. Given that a few-orbit exposure with the HST-WFPC-2 reveals about ten strong lensing candidate features (such as arclets; multiply-imaged galaxies) in a strong cluster (e.g., A370 – see Kneib et al. 1993; A2218, Kneib et al. 1995, 1996; MS1512, Seitz et al. 1998), it is clear that a moderately long exposure with NGST will probably detect of order one hundred such strong lensing features; and probably also more reliably than with WFPC-2, due to the better angular resolution which is needed to compare candidate multiple images by their morphology. Also here, multi-color images will be tremendously helpful. With these numerous strong lensing constraints in a single cluster, the projected mass distribution of these clusters can be determined with unprecedented spatial resolution, and even very small subcomponents will be detectable. Fig.1 provides a hint of how strong cluster lensing might appear with NGST. In addition, each strong lensing cluster will have a few highly magnified galaxy images, so that the already truly impressive light-collecting power of NGST can be coupled with these natural telescopes to map even fainter galaxies. The ‘transition zone’ between strong and weak lensing, in which hundreds of arclets will be found, can be used to obtain redshift estimates from the degree of their distortions, thus providing an independent means to measure the redshifts of the faintest galaxies observable with NGST (see, e.g., Kneib et al 1994; Ebbels et al. 1996, 1998).

The detailed mass models of clusters over a broad range of redshifts, and its comparison with other observables (such as X-ray emission, SZ-depletion, and galaxy distribution) will permit a thorough study of the relation between the dark and the baryonic matter in clusters. Questions like the validity of hydrostatic equilibrium of intra-cluster gas, the gas-to-mass fraction as a function of cluster mass and redshift, the possible presence of non-thermal pressure etc. can be investigated in great detail.

Clusters with such a large number of strong lensing features also provide a direct and purely geometrical handle on cosmological parameters, again through the dependence of the lensing strength on  $D_{\text{ds}}/D_{\text{s}}$  (e.g., Link & Pierce 1998). Whereas this method could in principle also be applied to current observations of multiple strong lensing features in clusters, most of the strong lensing features are too faint to obtain a reliable redshift, and in addition, one can also trade details of the mass distribution for changes in  $D_{\text{ds}}/D_{\text{s}}$ . This will not be the case if the number of strong lensing features becomes much larger.

**References:**

- Blandford, R.D., Saust, A.B., Brainerd, T.G. & Villumsen, J.V. 1991, MNRAS 251, 600.  
Brainerd, T.G., Blandford, R.D. & Smail, I. 1996 ApJ 466, 623.  
Ebbels, T.M.D. et al. 1996, MNRAS 281, L75.  
Ebbels, T.M.D. et al. 1998, MNRAS 295, 75.  
Geiger, B. & Schneider, P. 1998a, MNRAS 295, 497.  
Geiger, B. & Schneider, P. 1998b, MNRAS, submitted.  
Griffiths, R.E., Casertano, S., Im, M. & Ratnatunga, K.U. 1996, MNRAS 282, 1159.  
Hoekstra, H., Franx, M., Kuijken, K. & Squires, G. 1998, ApJ in press, also astro-ph/9711096.  
Hogg, D.W., Blandford, R.D., Kundic, T., Fassnacht, C.D. & Malhotra, S. 1996, ApJ 467, L73.  
Hudson, M.J., Gwyn, S.D.J., Dahle, H. & Kaiser, N. 1998, ApJ, in press, also astro-ph/9711341.  
Jain, B. & Seljak, U. 1997, ApJ 484, 560.  
Jain, B., Seljak, U. & White, S.D.M. 1998, astro-ph/9804238.  
Kaiser, N. 1992, ApJ 388, 272.  
Kaiser, N. 1998, ApJ 498, 26.  
Kaiser, N. & Squires, G. 1993, ApJ 404, 441.  
Kneib, J.-P., Mellier, Y., Fort, B. & Mathez, G. 1993, A&A 273, 370.  
Kneib, J.-P., Mathez, G., Fort, B., Mellier, Y., Soucail, G. & Longaretti, P.-Y. 1994, A&A 286, 701.  
Kneib, J.-P. et al. 1995, A&A 303, 27.  
Kneib, J.-P., Ellis, R.S., Smail, I., Couch, W.J. & Sharples, R.M. 1996, ApJ 471, 643.  
Kochanek, C.S. 1993, ApJ 419, 12.  
Kochanek, C.S. 1995, ApJ 453, 545.  
Kruse, G. & Schneider, P. 1998, MNRAS, submitted, also astro-ph/9806071.  
Link, R. & Pierce, M.J. 1998, astro-ph/9802207.  
Miralda-Escudé, J. 1990, 370, 1.  
Moore, B., Lake, G. & Katz, N. 1998, ApJ 495, 139.  
Natarajan, P. & Kneib, J.-P. 1997, MNRAS 287, 833.  
Natarajan, P., Kneib, J.-P., Smail, I. & Ellis, R.S. 1998, ApJ 499, 600.  
Ratnatunga, K.U., Ostrander, E.J., Griffiths, R.E. & Im, M. 1995, ApJ 453, L5.  
Rix, H.-W., Maoz, D., Turner, E.L. & Fukugita, M. 1994, ApJ 453, 49.  
Schneider, P. 1996, MNRAS, 283, 837.  
Schneider, P. 1998, ApJ 498, 43.  
Schneider, P. & Rix, H.-W. 1997, ApJ 474, 25.  
Schneider, P., van Waerbeke, L., Jain, B. & Kruse, G. 1998b, MNRAS 296, 873.  
Seitz, C., Kneib, J.-P., Schneider, P. & Seitz, S. 1996, A&A 314, 707.  
Seitz, C. & Schneider, P. 1995, A&A 297, 287.  
Seitz, S. & Schneider, P. 1996, A&A 305, 383.

Seitz, S. & Schneider, P. 1998, A&A, submitted.

Seitz, S., Saglia, R.P., Bender, R., Hopp, U., Belloni, P. & Ziegler, B. 1998, MNRAS, in press (also astro-ph/9706023).

Seljak, U. 1998, ApJ, in press, also astro-ph/9711124

Smail et al 1996, ApJ 469, 508.

Squires, G. et al. 1996a, ApJ 461, 572.

Squires, G., Kaiser, N., Fahlman, G., Babul, A. & Woods, D. 1996b, ApJ 469, 73.

Tormen, G., Diaferio, A. & Syer, D. 1998, MNRAS, in press.

Van Waerbeke, L. 1998, A&A 334, 1.

## ■ NGST Uniqueness/Relationship to Other Facilities

In this proposal, we shall exploit the by-far unique capability of NGST for weak gravitational lensing. The major advantages of NGST over other instruments for these studies are:

(1) Depth: the large aperture, combined with the largely reduced sky background, allows the imaging of much fainter galaxies than currently feasible. This will lead to a much larger number density  $n$  of galaxy images which can be used for these studies. Given that the intrinsic ellipticity distribution of galaxies provides the fundamental limit to the accuracy of any mass measurement, the noise in mass determinations decreases like  $n^{-1/2}$ .

(2) Angular resolution: Since galaxies tend to become smaller with decreasing brightness, the number of galaxies that can be used for weak lensing studies depends on the angular resolution; only galaxies which are not significantly smaller than the size of the PSF can have a reliable shape measurement. The unique angular resolution of NGST will allow to measure the shapes of highest-redshift galaxies provided they are larger in extent than  $\sim 500h^{-1}$  parsec, all of which contribute to  $n$ . Hence, even if the 10-meter class ground-based telescopes will carry out imaging surveys at significantly fainter magnitudes than currently available, their use for the weak lensing studies as outlined above will be restricted due to the small size of the very faint galaxies compared to the ground-based PSF. In addition, sampling of the PSF is essential for measuring accurate image ellipticities. The expected superb image quality is of utmost importance.

(3) Wavelength range: Since NGST provides images in the NIR with comparable or larger depth than even the HDF, it maps the visual-to-red emission of high-redshift galaxies which is expected to be considerably more regular than the rest-frame UV radiation. Since the noise of mass measurements increases proportionally to the dispersion  $\sigma_\epsilon$  of the intrinsic ellipticities of the background galaxies, mass estimates obtained from typical NGST wavebands will be more accurate than from optical telescopes.

(4) Wide-angular field imaging: Nearly all applications of weak lensing depend on solid angle  $\omega_{\text{cam}}$  covered per exposure: for a given science goal, the total observing time scales like  $\omega_{\text{cam}}^{-1}$ . Compared to the WFC-part of the WFPC-2, the currently planned 8K camera provides a gain of a factor  $\sim 3.5$  in  $\omega_{\text{cam}}$ , and hardly any gain compared to the Advance Camera. However, *this is another one of the science cases where switching to a larger-size CCD mosaic would immediately reduce the requested time, or for given observing time, would*

*enable more ambitious science goals to be obtained.* E.g., switching to an 16K mosaic, such as soon will become routinely available for optical wavelength, would yield an advantage by a factor of  $\sim 14$  relative to the WFC.

## ■ Observing Strategy

The signal-to-noise ratio for the detection of a mass concentration at redshift  $z_d$ , and thus the accuracy with which its mass and its mass profile can be measured, depends on the number density  $n$  of background galaxies, their redshift distribution and the dispersion  $\sigma_\epsilon$  of their intrinsic ellipticity distribution, and on the mass of the lens. The following estimate should indicate the required depth and field coverage for weak lensing studies, although the actual quantitative analysis will be carried out with more specialized tools.

Provided the lens can be described as an isothermal sphere with velocity dispersion  $\sigma_v$ , an ‘optimized’ statistics for their detection would be

$$X \propto \sum_i \frac{\epsilon_{ti}}{\theta_i},$$

where  $\theta_i$  is the separation of a background galaxy relative to the center of the foreground mass, and  $\epsilon_{ti}$  is the tangential component of the image ellipticity (see, e.g., Schneider 1996). The sum extends over all background galaxies within an annulus  $\theta_1 \leq \theta \leq \theta_2$ , where the inner radius is constrained by the ability to measure ellipticities reliably for images very close to the foreground galaxy (or, in the case of clusters, where the isothermal assumption breaks down due to flattening of the mass profile near the center), and the outer radius is determined either by considering neighboring foreground galaxies, or the decline of the mass profile relative to an isothermal profile. The signal-to-noise ratio of this statistics can be calculated to be

$$\frac{S}{N} = 12.7 \left( \frac{n}{30 \text{arcmin}^{-2}} \right)^{1/2} \left( \frac{\sigma_\epsilon}{0.2} \right)^{-1} \left( \frac{\sigma_v}{600 \text{km/s}} \right)^2 \left( \frac{\ln(\theta_2/\theta_1)}{\ln(10)} \right)^{1/2} \left\langle \frac{D_{ds}}{D_s} \right\rangle,$$

where  $D_{ds}$  and  $D_s$  are the angular-diameter distances from the lens and the observer to the source, respectively (the ratio  $D_{ds}/D_s$  is set to zero for galaxies with smaller redshift than the lens).

**(A) Determining the statistical properties of the dark matter halos of galaxies:** Statistically combining  $N_f$  similar foreground galaxies,  $S/N \propto N_f^{1/2}$ , so that for a given S/N, one needs

$$N_f = 350 \left( \frac{S/N}{10} \right)^2 \left( \frac{n}{600 \text{arcmin}^{-2}} \right)^{-1} \left( \frac{\sigma_\epsilon}{0.2} \right)^2 \left( \frac{\sigma_v}{150 \text{km/s}} \right)^{-4} \left( \frac{\ln(\theta_2/\theta_1)}{\ln(10)} \right)^{-1} \left( \frac{\langle D_{ds}/D_s \rangle}{0.15} \right)^{-2}$$

( $D_{ds}/D_s = 0.15$  in an EdS-Universe for  $z_d = 3$  and  $z_s = 5$ ). Extrapolating the current number counts in the K-band to  $K = 29$  yields a number density of  $\sim 5 \times 10^6 \text{deg}^{-2}$ ; allowing for a flattening of the counts for fainter magnitudes, as perhaps expected from theoretical

models, the fiducial number density of background galaxies may be realistic for images down to  $K \sim 29$ , which would have a broad redshift distribution extending to far beyond  $z = 5$ .

Investigating galaxies at  $K \sim 24$  which will cover a broad redshift range  $1 \lesssim z \lesssim 5$  and which have a surface number density of  $\sim 4 \times 10^5 \text{mag}^{-1} \text{deg}^{-2}$ , and splitting these galaxies into bins of width  $\Delta z = 0.1$  and  $\Delta K = 0.1$  to define ‘similar galaxies’, we obtain about  $10^3$  galaxies per bin and per  $\text{deg}^{-2}$ . Of course, different binning is also possible, e.g., with larger  $\Delta z$  (related to the accuracy of photometric redshift estimates) and according to morphology or color. In any case, the assumption of about 200 bins is physically meaningful. Thus, for the assumed fiducial parameters,  $0.2 \text{deg}^2$  are needed to obtain a  $S/N = 10$  in a typical bin (and thus to determine  $\sigma_v$  in this bin with an accuracy of  $\sim 5\%$ , or to investigate the radial dependence of the matter density). This requires about 40 pointings per filter, with an exposure time of 27600 seconds, assuming that the typical size of a  $K \sim 29$  galaxy is  $0''.3$  and should have a  $S/N$  of 5 to allow accurate shape determination. Together, this requires about 13 days of imaging in the K-band. In order to obtain accurate redshift estimates from multiband photometry, the same fields should be imaged in at least 4 other bands (e.g., V,I,H,M) with about the same observing time; this should guarantee the availability of a redshift estimate for the majority of all galaxies used in the analysis, given that lower  $S/N$  in the other bands are acceptable.

**(B) Determining the masses of high-redshift clusters/groups:** Scaling the previous  $S/N$ -estimates to clusters,

$$\frac{S}{N} = 5.6 \left( \frac{n}{300 \text{arcmin}^{-2}} \right)^{1/2} \left( \frac{\sigma_\epsilon}{0.2} \right)^{-1} \left( \frac{\sigma_v}{500 \text{km/s}} \right)^2 \left( \frac{\ln(\theta_2/\theta_1)}{\ln(10)} \right)^{1/2} \left( \frac{\langle D_{\text{ds}}/D_s \rangle}{0.2} \right),$$

we see that halos with  $\sigma_v \gtrsim 500 \text{km/s}$  can be significantly detected, provided their redshift is not much larger than about 3; more massive halos will be detected at accordingly higher redshift. For  $S/N \gtrsim 10$ , detailed studies of their projected mass distribution are possible (radial mass profile, substructure, etc.). To obtain an accurate estimate of the total mass, fields of at least  $8'$  (or  $\sim 2h^{-1} \text{Mpc}$  sidelength) around the cluster ‘center’ are required (with the ACS it will be possible to obtain detailed mass maps near the center of lower- $z$  clusters, but for the outer part, the signal is too weak to be measured reliably – the much higher number density of background galaxies is essential for that). Selecting 50 clusters from a sample of candidates up to  $z \sim 2.5$ , requiring 4 pointings per cluster and about 5000 seconds exposure time to reach  $K \sim 27.5$  (assuming a typical size of  $0''.5$ ), 12 days per filter are required; with  $K \sim 27.5$ , a number density of  $n \sim 300 \text{arcmin}^{-2}$  will be reached with is the density needed to measure a shear of  $\sim 2\%$  – expected at 4 arcminutes from a typical massive cluster at  $z \sim 1$  – in  $1 \text{arcmin}^2$  bins with a 50% accuracy. With the same arguments as in (A) above, to obtained photometric redshifts estimates, about the same exposure time for four other bands are required, yielding a total integration time of 60 days.

**(C) Measuring the statistical properties of the dark matter distribution in the Universe:** To obtain an accurate view of the mass inventory of the Universe up to redshifts of  $\sim 3$ , 10 fields of total area  $\sim 5 \text{deg}^2$  shall be mapped down to  $K \sim 26.8$ , i.e., with 20 minutes exposures. This will allow to measure the statistical properties of the dark matter

distribution up to  $z \sim 3$ , and at the same time will give a significant sample of mass-selected halos with  $\sigma_v \gtrsim 500\text{km/s}$ , this limit depending on halo redshift. Depending on cosmology, a sample of  $\gtrsim 500$  mass-selected clusters will be obtained. The total integration time needed is  $\sim 13.4$  days per filter. In order to ‘slice’ through redshift space, using the redshift dependence of the lensing effect, photometric redshifts are essential, so that four additional bands with the same exposure time will be taken.

The distribution of the fields on the sky is to some degree arbitrary. To allow the measurements of coherent image distortion patterns over large areas as needed for cosmic shear measurements, and to avoid excessive ‘boundary effects’ in the cluster finding procedure, however, the pointings of the WFIS should be organized in larger patterns. In addition, studies of galaxy-galaxy lensing are strongly assisted if a relatively large consecutive area around the lines-of-sight probed is available. We therefore propose to distribute the fields of the VDIS and the WFIS over 10 high-latitude directions. At the center of each such patch, an  $8 \times 8$  arcminute field of the VDIS is located, surrounded by a  $40 \times 40$  arcminute field of the WFIS. Hence, each patch requires 4 pointings in the VDIS, and 96 pointings (all per waveband) for the WFIS.

If the images are taken on several visits, separated by timescales of weeks or months, they can be used to search for variable or transient events, such as high-galactic latitude variable stars, proper motions, or very high-redshift supernovae.

## ■ Special Requirements

To allow for accurate CR removal, every science exposure should be split in at least 4 subexposures. For the WFIS, this leads to an exposure time per frame of 5 minutes. Assuming an 8K-camera and 4 bytes/pixel to allow for sufficient dynamic range (galaxies with K-magnitudes between  $\sim 20$  and  $\sim 29$  should be equally covered), this yields a data flow rate of about 60 Gb/day. If the WFIS exposures are interchanged with those of the VDIS, this requirement becomes less strong. However, even for the VDIS, individual exposures should not be much longer than 5 minutes to obtain high dynamic range; a further argument for short individual exposures in the strategy of repeated visits to look for transients. On-board CR removal and coaddition of the individual exposures can ease the pressure on the data flow rate.

Minimum science data volume: 20 GB/day or observation

Minimum precision/pixel dynamic range: 64000

## ■ Precursor/Supporting Observations

Dark matter concentrations found in the WFIS are expected to be clusters/proto-clusters at redshifts up to  $z \sim 3$ , with more typical values of  $z \sim 2$  or slightly lower. To verify the nature of these dark halos as genuine clusters, spectroscopy of the galaxies in the field has to be performed. A massive spectroscopic follow-up program in the field of cluster candidates at 10-meter class telescopes will be needed to reveal the physical nature of these mass concentrations and to measure the redshifts of arcs and multiply-imaged background

galaxies. In addition, pointed X-ray observations would support their physical interpretation. Ground-based imaging with 10-m class telescopes can supplement the proposed imaging with NGST in obtaining deep wide-field U and B-band, or deep narrow-band images. Selection of the high galactic latitude ‘random’ fields can be made on the basis of then existing deep imaging observations in other wavebands (e.g., far IR, sub-mm/mm, X-ray).

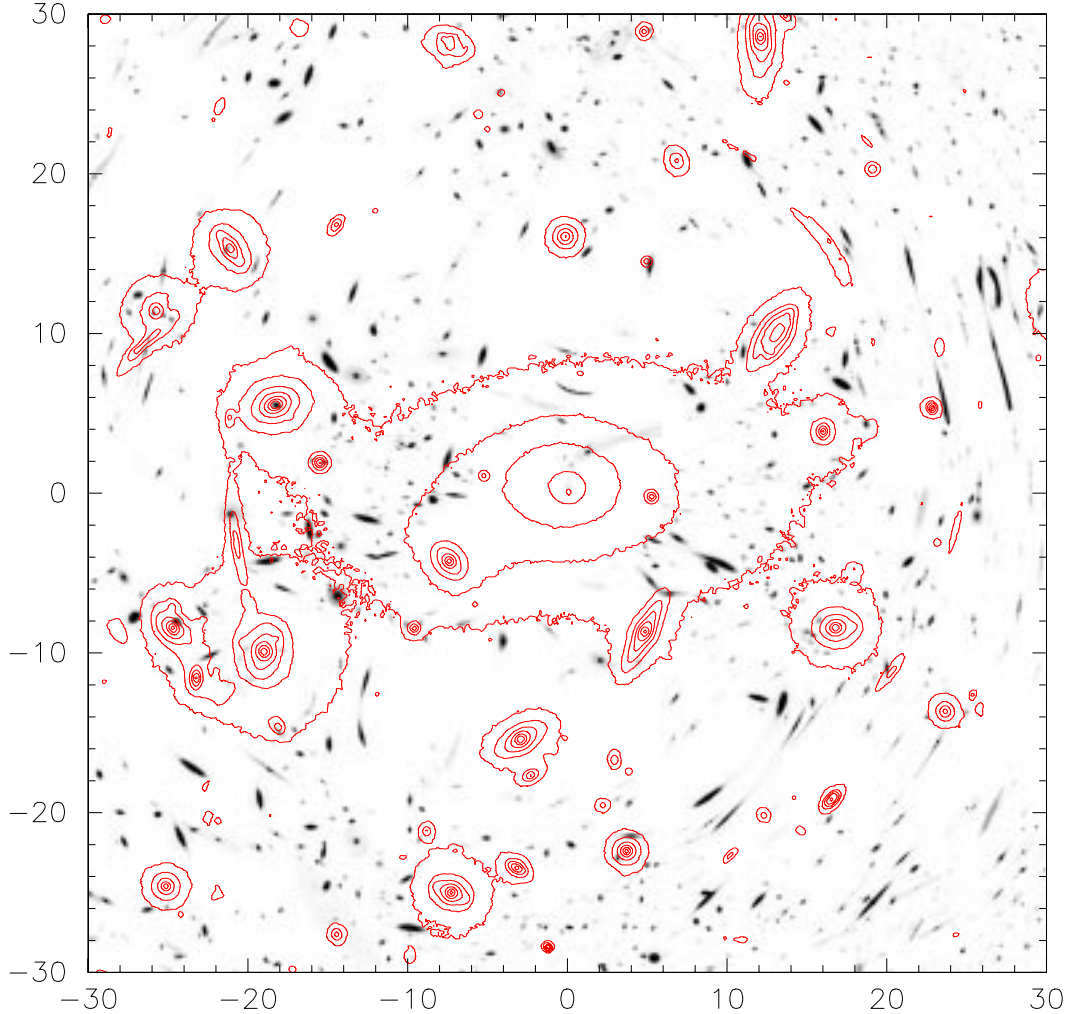


Figure 1: *Simulated image of lensed features in the very central part of the massive cluster A2218. For these simulations, the mass profile of the cluster as constrained from HST observations and detailed modelling (Kneib et al 1996) has been used. The galaxy population model used in this simulation is somewhat simple (and likely to be highly oversimplified at such faint magnitudes). The number density of (unlensed) sources was assumed to be  $4 \times 10^6 \text{deg}^{-2}$  down to  $K=29$ . To determine the physical quantities like absolute magnitude and intrinsic size, we applied the  $K+e$  correction from Bruzual and Charlot (1993) galaxy synthesis model. To match current observations, we also include a size-dependence with redshift. The redshift distribution assumed is broad and extend to redshift  $z \sim 10$  with a median value  $z_{\text{med}} \sim 3$ . The brighter objects (cluster galaxies and brightest arcs) seen by HST are displayed as contours, to make the faint galaxy images visible on this limited dynamic range reproduction. An enormous number of large arcs and arclets are seen; in particular, numerous radial arcs can be easily detected, which will allow to determine the ‘core size’ of the cluster mass distribution. Due to the broad redshift distribution of the faint galaxies, arcs occur at quite a range of angular separations from the cluster center; this effect will become even stronger for higher-redshift clusters. It should be noted that this 1 arcminute field does not cover the second mass clump seen with HST; an NGST image will cover a much larger area, and more strong lensing features will be found which can then be combined with the weak lensing analysis of such a cluster. For this simulation we have used a 0.06 arcsecond pixel size; the NGST sampling will be better by a factor of 2.*